Redox Biology 69 (2024) 102999

Contents lists available at ScienceDirect

Redox Biology

journal homepage: www.elsevier.com/locate/redox

Cysteine and homocysteine can be exploited by GPX4 in ferroptosis inhibition independent of GSH synthesis

Chaoyi Xia [b], Xiyue Xing [b], Wenxia Zhang [b], Yang Wang [b], Xin Jin [b], Yang Wang [b], Meihong Tian [a,**], Xueqing Ba [b,***], Fengqi Hao [a,b,*,1]

[a] School of Physical Education, Northeast Normal University, 5268 Renmin Street, Changchun, Jilin, 130024, China
[b] Key Laboratory of Molecular Epigenetics of Ministry of Education, Northeast Normal University, Changchun, Jilin, 130024, China

ARTICLE INFO

Keywords:
Cysteine
Homocysteine
GSH
Glutathione peroxidase 4
Ferroptosis

ABSTRACT

Ferroptosis is inhibited by glutathione peroxidase 4 (GPX4), an antioxidant enzyme that uses reduced glutathione (GSH) as a cofactor to detoxify lipid hydroperoxides. As a selenoprotein, the core function of GPX4 is the thiol-dependent redox reaction. In addition to GSH, other small molecules such as cysteine and homocysteine also contain thiols; yet, whether GPX4 can exploit cysteine and homocysteine to directly detoxify lipid hydroperoxides and inhibit ferroptosis has not been addressed. In this study, we found that cysteine and homocysteine inhibit ferroptosis in a GPX4-dependent manner. However, cysteine inhibits ferroptosis independent of GSH synthesis, and homocysteine inhibits ferroptosis through non-cysteine and non-GSH pathway. Furthermore, we used molecular docking and GPX4 activity analysis to study the binding patterns and affinity between GPX4 and GSH, cysteine, and homocysteine. We found that besides GSH, cysteine and homocysteine are also able to serve as substrates for GPX4 though the affinities of GPX4 with cysteine and homocysteine are lower than that with GSH. Importantly, GPX family and the GSH synthetase pathway might be asynchronously evolved. When GSH synthetase is absent, for example in *Flexibacter*, the fGPX exhibits higher affinity with cysteine and homocysteine than GSH. Taken together, the present study provided the understanding of the role of thiol-dependent redox systems in protecting cells from ferroptosis and propose that GSH might be a substitute for cysteine or homocysteine to be used as a cofactor for GPX4 during the evolution of aerobic metabolism.

1. Introduction

Ferroptosis is a regulated form of cell death caused by iron-dependent peroxidation of polyunsaturated phospholipids (PUFA-PLs) on cell membranes [1,2]. It has been emerging as a novel mode of cell death and is strongly associated with neurodegenerative diseases and ischemic injury; while inducing ferroptosis in tumor cells contributes to cancer treatment [3,4]. Cyst(e)ine/glutathione (GSH)/glutathione peroxidase 4 (GXP4) is the primary system that prevents ferroptosis [5]. Mechanistically, GPX4 converts lipid hydroperoxides to lipid alcohols using GSH as a cofactor [6]. The antioxidant GSH is a tripeptide synthesized from glutamate, cysteine, and glycine. The synthesis of GSH is divided into two steps [7]. In the first step, glutamate and cysteine are joined by the catalytic subunit of glutamate-cysteine ligase (GCLC), producing the dipeptide γ-glutamyl-cysteine (γ-Glu-Cys). Next, glutathione synthase (GSS) adds glycine to γ-Glu-Cys, generating the tripeptide GSH (γ-Glu-Cys-Gly). For generation of GSH, cysteine reduced from cystine is the rate-limiting precursor [8]. Most cells obtain cystine primarily through the solute carrier family 7 member 11 (SLC7A11, also known as xCT) [9], an amino acid antiporter that mediates the transmembrane exchange of extracellular cystine and intracellular glutamate across the cell membrane [10,11]. Based on this, cystine depletion in the medium and treatment with the inhibitor of xCT (e.g., erastin or IKE), are categorized as the class 1 ferroptosis inducers (FINs) [12,13]; while GPX4 inhibitors (e.g., RSL3) are taken as the class 2 FINs [6,12].

Although the GSH is necessary for GPX4 activity, Brugge et al. reported unexpected responses of cancer cells to the inhibition of GSH synthesis by L-buthionine sulfoximine (BSO), an inhibitor of GCLC. GSH

* Corresponding author. School of Physical Education, Northeast Normal University, 5268 Renmin Street, Changchun, Jilin, 130024, China.
** Corresponding author.
*** Corresponding author.
E-mail addresses: tianmh749@nenu.edu.cn (M. Tian), baxq755@nenu.edu.cn (X. Ba), haofq340@nenu.edu.cn (F. Hao).
[1] Lead contact: Fengqi Hao.

https://doi.org/10.1016/j.redox.2023.102999
Received 22 November 2023; Received in revised form 14 December 2023; Accepted 14 December 2023
Available online 22 December 2023

depletion could only result in a delayed cytotoxic phenotype, manifesting as apoptosis in UACC-812, MDA-MB-361, and T-47-D cells; whereas, the vitality of HCC-1806, MDA-MB-468 and MDA-MB-231 cells was scarcely changed [14]. In addition, DeNicola et al. observed that BSO treatment could not induce ferroptosis in A549 and Calu3 cells [15]. Cyst(e)ine/GSH/GXP4 plays a critical role in ferroptosis prevention. However, while deprivation of cysteine can inhibit GPX4 activity and significantly induce ferroptosis, blocking the synthesis of GSH with BSO can not. This strongly suggests that there are other backup mechanisms to support GPX4 function in the regulation of ferroptosis in the absence of GSH.

The critical function of GPX4 is the thiol-dependent redox reaction. In addition to GSH, cysteine and homocysteine also have thiols [16], and homocysteine can be converted to cysteine through the transsulfuration pathway [17]. Intriguingly, Takahashi et al. showed that some isoforms of mammalian GPXs can utilize small molecules containing thiol groups, such as GSH, dithiothreitol, mercaptoethanol, and cysteine as substrates to remove hydrogen peroxide (H_2O_2) in vitro [18]. This study suggested that once the cellular GSH supply is defective, thiol moieties of cysteine and homocysteine might be directly exploited to detoxify lipid hydroperoxides and inhibit ferroptosis. The roles of cysteine and homocysteine in regulation of ferroptosis are plausible and need to be clarified.

In the present study, we show that ferroptosis can be alleviated by administration of cysteine and homocysteine while endogenous GSH synthesis was blocked, and these thiol-containing small molecules inhibited ferroptosis in a GPX4-dependent manner. The GPX from GSH-absent lower species, such as *Flexibacter*, exhibited higher affinity with cysteine and homocysteine than GSH, suggesting that using GSH as a cofactor of GPX4 might be an evolutionary selection from other thiol-containing molecules such as cysteine and homocysteine.

2. Materials and methods

2.1. Cell culture

HT1080 human fibrosarcoma (HT1080) cells, mouse embryo fibroblasts (MEFs) and A549 cells were obtained from the American Tissue Culture Collection (ATCC). Cells were cultured at 37 °C, 5 % CO_2 in Dulbecco's Modified Eagle's medium (DMEM) without L-methionine, L-cystine, and L-glutamine (D0422, Sigma), supplemented with 10 % fetal bovine serum and 1 % penicillin/streptomycin. Based on different experimental designs, cells were kept in medium containing cystine (1161586, Sigma), homocysteine (H4628, Sigma), cystathionine (C7505, Sigma), L-homocystine (H6010, Sigma), D-homocystine (H5134, Sigma), methionine (M0960000, Sigma), glutamine (1294808, Sigma), BSO (S9728, Selleck), RSL3 (S8155, Selleck), ferrostatin-1 (Fer-1) (S7243, Selleck), deferoxamine (DFO) (Y0001937, Sigma), DL-propargylglycine (PAG) (P7888, Sigma) or sodium hydrosulfide (NaHS) (161527, Sigma).

2.2. Lipid ROS detection

According to the previous descriptions [19,20], 4 μM BODIPY 581/591C11 (D3861, ThermoFisher) was added into cell culture medium and incubated for 25 min. Then, cells were collected and subjected to assessment of lipid ROS. Cells positive for BODIPY 581/591C11 were defined as lipid ROS accumulation. Flow cytometry analysis was carried out with BD FACS Canto II flow cytometer (BD Biosciences), and acquired data were analyzed using FlowJo, version 10, software (FlowJo).

2.3. Cell death measurement

To analyze cell death, cells were collected and stained with propidium iodide (PI) (P4170, Sigma) according to the previously described [19,20]. Dead cells were detected by flow cytometry analysis and defined by positive for PI staining.

2.4. ROS analysis

For ROS detection, 10 μM DCFH-DA (35845, Sigma) was added into cell culture medium. After 30 min incubated, cells were collected and subjected to assessment of ROS by flow cytometry analysis.

2.5. Glutathione assay

The level of glutathione was measured with glutathione reductase coupled reaction using Glutathione Assay Kit (S0053, Beyotime) according to the kit instructions. Briefly, deproteinated cell lysates and the standard with different concentrations were respectively mixed with the Assay Cocktail regent containing glutathione reductase, NADPH, and DTNB. The GSH of this reaction included both the intrinsic GSH and the reduction of GSSG by glutathione reductase. The thiol group of GSH reacted with DTNB and produced a yellow colored TNB. In addition, the mixed disulfide, GSTNB (between GSH and TNB) that was concomitantly produced, was also reduced by glutathione reductase to recycle the GSH and produced more TNB. Measurement of the absorbance of TNB at 405 nm was directly proportional to the concentration of GSH + GSSG, which was normalized with the same cell number of each sample.

2.6. Cysteine analysis

The assessment of cysteine content was performed with Cysteine Content Assay Kit (D799571, Sangon Biotech) according to the manufacturer's instructions. In brief, cells were collected and subjected to cysteine extraction. The extraction sample, as well as the standard solution with different concentrations were respectively mixed with reaction buffer containing the critical reagent, phosphotungstic acid. Cysteine, exited in the extraction sample or standard solution, could reduce the phosphotungstic acid to produce tungsten blue, which has an absorption peak at 600 nm. The content of cysteine can be calculated with the absorbance at 600 nm and normalized with the same cell number of each sample.

2.7. Real-time PCR

Total RNA was isolated using TRNzol (DP424, TIANGEN). cDNA was synthesized with the PrimeScript RT reagent Kit plus gDNA Eraser (RR047A, TaKaRa) according to manufacturer's instructions. Real-time PCR was performed on the QuantStudio 3 real-time PCR instrument (Applied Biosystems) with a TB Green Premix Ex Taq (Tli RNase H Plus) regent (RR820A, TaKaRa). The mRNA expression of genes was normalized to the expression of β-actin gene. Data were analyzed using the comparative cycling threshold method. The sequences of the primers used for real-time PCR were: *prostaglandin-endoperoxide synthase-2* (*Ptgs2*) (Mouse), forward TGAGCAACTATTCCAAACCAGC, reverse GCACGTAGTCTTCGATCACTATC; *ACTB* (Mouse), forward GGCTGT ATTCCCCTCCATCG, reverse CCAGTTGGTAACAATGCCATGT.

2.8. siRNA knockdown

Transfections were carried out using Lipofectamine 2000 Transfection Reagent (11668019, Invitrogen) according to the manufacturer's instructions. After transfection, cells were cultured for 48 h and then were collected for evaluating the interference efficiency using Western blot. The oligonucleotides for knockdown were listed as followed: CBS1-AGACGGAGCAGACAACCUAT, CBS2-CACCACCGCUGAUGAGAUCTT, CBS3-GGACGGCGGCGGACAAGUGTT; GCLC1-GGAGGAAACCAAGCGCCAUTT, GCLC2- GCUCUUUGCACAAUAACUUTT, GCLC3-GCAUGUUGCUCAUCUCUUUTT; negative control (NC)- UUCUCCGAACGUGUCACGUUTT.

2.9. Overexpression of xCT

For overexpression of xCT, the gene was cloned in the pcDNA3.1-3 × Flag vector to generate the recombinant pcDNA3.1-3 × Flag-xCT. Next, HT1080 cells were transduced with pcDNA3.1-3 × Flag-xCT using Lipofectamine 2000 Transfection Reagent according to the protocol recommended by the manufacturer. Following transduction for 24 h, cell lysates were analyzed for Flag-xCT expression with Western blot using antibody against Flag.

2.10. Western blot

Cell lysate preparation, SDS-PAGE, and electrophoretic transference were accomplished as previously described [21]. Membranes were blocked with 5 % (wt/vol) nonfat dried milk in TBS (pH 7.2) containing 0.1 % Tween 20 (TBST) and incubated with the appropriate antibodies in 5 % (wt/vol) nonfat dried milk in TBST overnight at 4 °C. The following primary antibodies were used: anti-GCLC (1:1000) (A1038, ABclonal), anti-MAT2A (1:1000) (A19272, ABclonal), anti-SAHH (1:1000) (A2756, ABclonal), anti-CBS (1:1000) (A11612, ABclonal), anti-CTH (1:1000) (A6121, ABclonal), and anti-β-actin (1:1000) (HC201-01, TransGen Biotech). All primary antibody incubations were followed by incubation with secondary HRP-conjugated antibody in 5 % (wt/vol) nonfat dried milk in TBST and visualized using chemiluminescent HRP substrate on chemiluminescence image system (Tanon Science and Technology Company).

2.11. Molecular docking analysis

Firstly, the protein sequence of human GPX4 or *Flexibacter* GPX were constructed full-length structure (initial structure) using AlphaFold2 [22]. Secondly, the initial structure was processed by AutoDock Tools 1.5.6 [23] to retain the original charge of the protein and generate a pdbqt file for molecular docking analysis. Thirdly, using MOPAC program to optimize the molecular structure of GSH, cysteine, and homocysteine and calculate the atomic charge of PM3 [24], and using AutoDock Tool 1.5.6 to generate relevant pdbqt files for molecular docking analysis. Finally, the AutoDock 4.2.6 software package and Amber14 force field were used to perform and optimize the molecular docking analysis [25].

2.12. Glutathione peroxidase activity assay

Mouse liver homogenates were used to evaluate glutathione peroxidase activity in response to GSH (0.25 mM), cysteine (0.25 mM) or homocysteine (0.25 mM), respectively. The activity of glutathione peroxidase was measured using the Cellular Glutathione Peroxidase Assay Kit with DTNB (S0057S, Beyotime) according to the manufacturer's guidance.

2.13. Intracellular hydrogen sulfide detection

For intracellular hydrogen sulfide (H_2S) measurement, cells were collected and stained with 10 μM H_2S fluorescent probe (MX5302, Maokang Biotechnology) according to the manufacturer's instructions. After 30 min staining, the levels of H_2S were detected by flow cytometry analysis.

2.14. Statistical analysis

Statistical analysis was performed using GraphPad Prism, version 8.3.0. Data are displayed as mean ± SD. Difference between two groups was analyzed by *t*-test. One-way ANOVA was performed when more than two groups were compared. The values of $P < 0.05$ were considered significant. P values are indicated on graphs as $^{*}P < 0.05$, $^{**}P < 0.01$, $^{***}P < 0.001$, and $^{****}P < 0.0001$.

3. Results

3.1. Cysteine is capable to inhibit ferroptosis independent of GSH synthesis

Cyst(e)ine/glutathione (GSH)/glutathione peroxidase 4 (GXP4) is the main system in the prevention of ferroptosis [5,6]; however, a recent study found that depletion of GSH by the glutamate-cysteine ligase catalytic subunit (GCLC) inhibitor L-buthionine sulfoximine (BSO) did not significantly induce ferroptosis [15]. Failure of GSH synthesis is evidently linked to the persistence of cellular cysteine, this prompted us to hypothesize that cysteine might backup GPX4 function in ferroptosis inhibition. To test , mouse embryo fibroblasts (MEFs) were subjected to ferroptosis induction via cystine deprivation, and along with cystine concentration descending, intracellular GSH gradually decreased (Fig. 1 A); correspondingly, lipid ROS (a hallmark of ferroptosis) accumulation increased (Fig. 1 B and Fig. S1 A). Ferroptosis was detected by propidium iodide (PI) staining (Fig. 1C and Fig. S1 B), which were abrogated by the treatment of ferroptosis inhibitor (Fer-1 and DFO) (Fig. 1 B and Fig. S1 A; Fig. 1C and Fig. S1 B). In addition, the accumulation of lipid ROS and cell death induced by cystine deprivation were also observed in A549 cells (Fig. S1 C and D). These results validated the important role of cyst(e)ine/GSH/GPX4 axis in combating ferroptosis.

Next, HT1080 human fibrosarcoma (HT1080) cells and MEFs were treated with BSO to block intracellular GSH synthesis (Fig. 1 D and E), however, the depletion of GSH failed to upregulate lipid ROS levels (Fig. 1 F and Fig. S1 E; Fig. 1 G and Fig. S1 G), correspondingly, the cell death was undetectable (Fig. 1H and Fig. S1 F; Fig. 1 I and Fig. S1 H). Likewise, we also found that the inhibition of GSH synthesis did not trigger lipid ROS accumulation and cell death in A549 cells (Fig. S1 I-K). Furthermore, we designed siRNA targeting GCLC, a key enzyme of the GSH synthesis, to downregulate GCLC expression in HT1080 cells (Fig. S1 L), and to block intracellular GSH synthesis (Fig. S1 M). We found that neither lipid ROS level (Fig. 1 J and Fig. S1 N) nor cell death (Fig. 1 K and Fig. S1 O) were induced by knockdown of GCLC. Notably, the inhibition of GSH synthesis caused a significant accumulation of intracellular cysteine in HT1080 cells and MEFs (Fig. 1 L and M), that was comparable with the intrinsic GSH level. Taken together, our data indicated that deprivation of cysteine could cause depletion of intracellular GSH and result in ferroptosis; whereas, in the presence of cysteine, blocking the synthesis of GSH is insufficient to do so, suggesting the thiol group existing in cysteine might be exploited by GPX4 for anti-ferroptosis.

3.2. Homocysteine is capable to inhibit cystine deprivation-induced ferroptosis

Given that homocysteine is also an important intracellular small biomolecule containing thiol group, the impact of homocysteine on cystine deprivation-induced ferroptosis was detected. We observed that increasing homocysteine concentration in cell culture medium resulted in the gradual decline of lipid ROS (Fig. 2 A and Fig. S2 A) and cell death (Fig. 2 B and Fig. S2 B) induced by cystine deprivation in MEFs. Given that in the process of defending against ferroptosis, cysteine and cystine form an oxidation-reduction pair, we analyzed the inhibitory effect of homocystine on ferroptosis induced by cystine deprivation. As anticipated, treatment of L-homocystine inhibited lipid ROS accumulation induced by cystine starvation in HT1080 cells (Fig. 2C and Fig. S2 C); meanwhile, cell death induced by cystine starvation was also effectively prevented (Fig. 2 D and Fig. S2 D). Interestingly, while the inhibition of lipid ROS and cell death caused by L-homocystine treatment was comparable with cystine and homocysteine treatment (Fig. 2C and Fig. S2 C; Fig. 2 D and Fig. S2 D), D-homocystine failed to do so (Fig. 2C and Fig. S2 C; Fig. 2 D and Fig. S2 D), probably due to D-homocystine cannot be reduced to homocysteine in the cells. These results suggested the thiol group of homocysteine is indispensable for GPX4 in ferroptosis

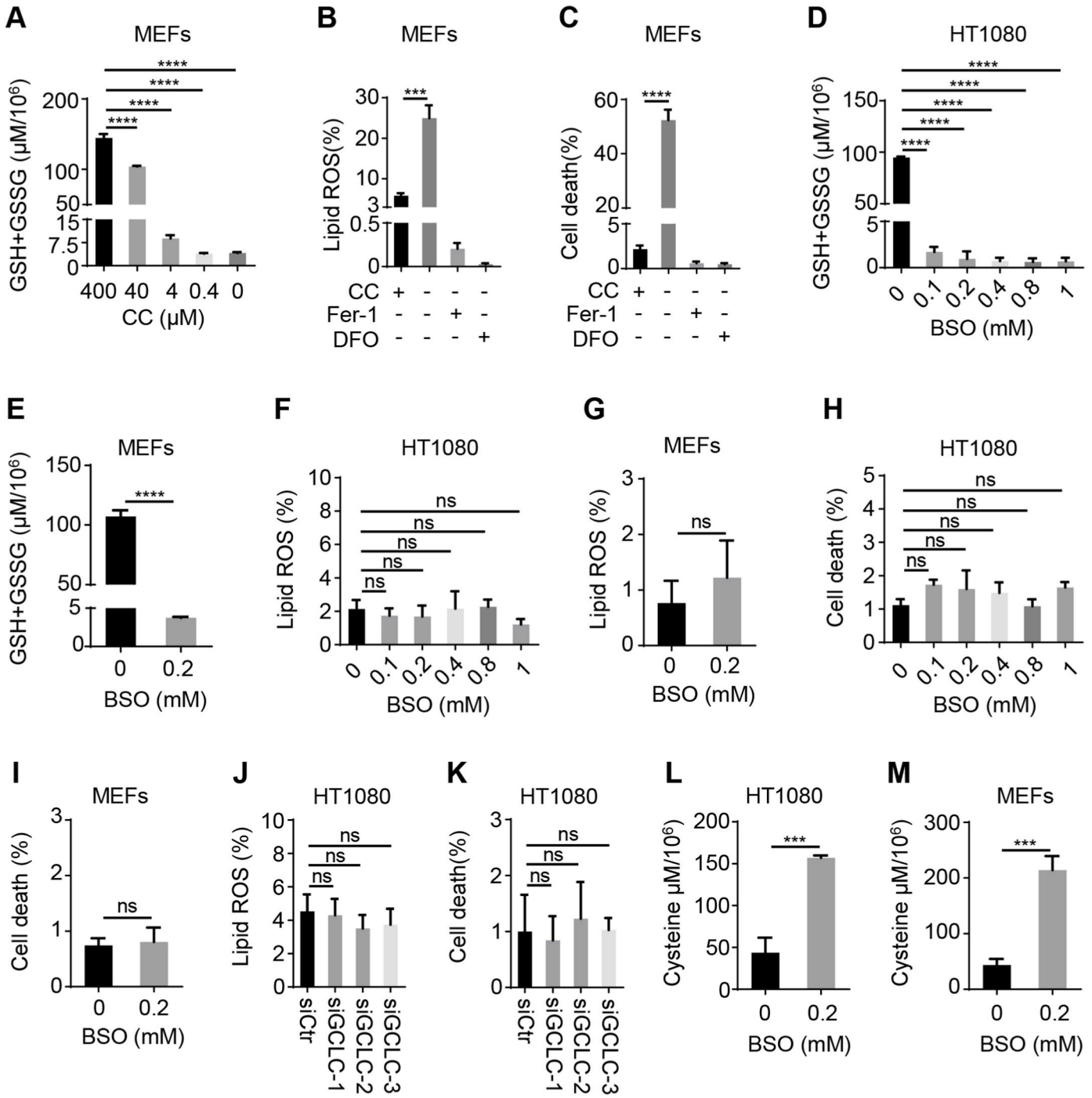

Fig. 1. Cysteine is capable to inhibit ferroptosis independent of GSH synthesis.
(A) Impact of cystine (CC) on glutathione (GSH) and oxidized glutathione (GSSG) level. MEFs were treated with indicated concentrations of CC for 8 h and subjected to assessment of GSH and GSSG level. (B and C) Analysis of lipid ROS level and cell death upon CC deprivation. MEFs were cultured in the absence or presence of CC (400 μM) for 8 h for evaluation of lipid ROS (B) or for 12 h for cell death detection (C). The lipid ROS accumulation or cell death were assessed by BODIPY 581/591C11 or propidium iodide (PI) staining coupled with flow cytometry analysis, respectively. Ferrastain-1 (Fer-1, 10 μM) and deferoxamine (DFO, 80 μM), two classical inhibitors of ferroptosis, were included as negative control. (D and E) Measurement of glutathione (GSH) and oxidized glutathione (GSSG) level upon impairment of GSH synthesis by L-buthionine sulfoximine (BSO). HT1080 cells (D) and MEFs (E) were cultured in the absence or presence of indicated amount of BSO for 24 h and subjected to assay of GSH and GSSG level. (F–I) Assay of lipid ROS level and cell death in the presence of BSO. Following treatment as described in Fig. 1 (D and E), HT1080 cells and MEFs were collected for assessment of lipid ROS (F and G) and cell death (H and I) as described in Fig. 1 (B and C). (J and K) Assessment of lipid ROS and cell death for GCLC-depleted cells. HT1080 cells were transfected with siRNA against GCLC or scramble for 60 h and subjected to measurement of lipid ROS (J) as described in Fig. 1 (B), and detection of cell death (K) as described in Fig. 1 (C). (L and M) Evaluation of intracellular cysteine level upon GSH inhibition. HT1080 cells and MEFs were cultured in the absence or presence of BSO (0.2 mM) for 24 h and subjected to detection of intracellular cysteine level. Data represent as mean ± SD of three independent experiments, with significance determined by one-way ANOVA test or t text. ***$P < 0.001$; ****$P < 0.0001$; ns, nonsignificant.

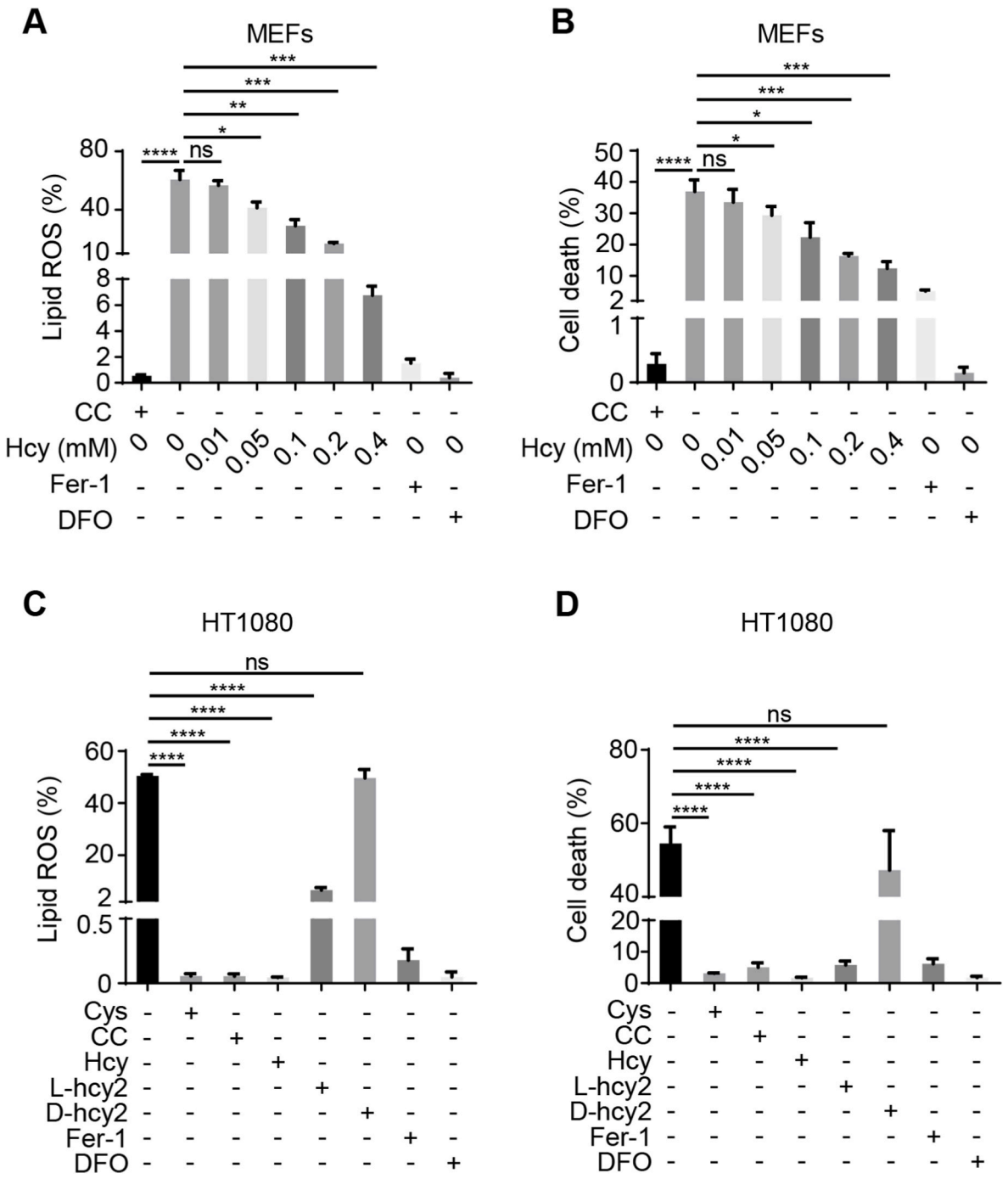

Fig. 2. Homocysteine is capable to inhibit cystine deprivation-induced ferroptosis.
(A and B) Assay for lipid ROS and cell death in response to homocysteine (Hcy) treatment in MEFs. In the absence of cystine (CC), MEFs were cultured with indicated concentrations of Hcy for 8 h for lipid ROS analysis (A) as described in Fig. 1 (B), or for 10 h for evaluation of cell death (B) as described in Fig. 1 (C). (C and D) Measurement of the impact of Hcy on lipid ROS and cell death. HT1080 cells were cultured in the absence or presence of cysteine (Cys, 400 μM), cystine (CC, 400 μM), homocysteine (Hcy, 400 μM), L-homocystine (L-hcy2, 400 μM), or D-homocystine (D-hcy2, 400 μM). Cells were incubated for 10 h for lipid ROS assessment (C) as described in Fig. 1 (B), or for 14 h for evaluation of cell death (D) as described in Fig. 1 (C). The presence of CC (400 μM) in Fig. 2 (A and B), Fer-1 (10 μM) or DFO (80 μM) in Fig. 2 (A–C) were the negative control. Data represent as mean ± SD of three independent experiments, with significance determined by one-way ANOVA test. $^{*}P < 0.05$; $^{**}P < 0.01$; $^{***}P < 0.001$; $^{****}P < 0.0001$; ns, nonsignificant.

prevention.

3.3. The role of homocysteine in ferroptosis inhibition is independent of transsulfuration pathway

Homocysteine can be converted into cysteine via the transsulfuration pathway that includes two steps. In the first step, serine and homocysteine are condensed to form cystathionine by cystathionine β-synthase (CBS). Next, cystathionine γ-lyase (CTH) cleaves the cystathionine molecule into cysteine, ammonia, and 2-oxobutanoate [17,26]. Therefore, whether the role of homocysteine in ferroptosis inhibition depends on the transsulfuration pathway was further investigated. We designed siRNA targeting CBS, a key enzyme of the transsulfuration pathway, to impair CBS expression in HT1080 cells (Fig. S3 A), and then

evaluate the inhibitory effect of homocysteine on ferroptosis upon the transsulfuration pathway was blocked. Our data showed that the downregulation of CBS expression did not compromise the inhibitory effect of homocysteine on cystine starvation-induced lipid ROS (Fig. 3 A and Fig. S3 B) and cell death (Fig. 3 B and Fig. S3 C), indicating the inhibitory effect of homocysteine on ferroptosis is independent on transsulfuration pathway. More importantly, we found that CBS is abundantly expressed in HT1080 cells, whereas almost undetectable in MEFs (Fig. S3 D), indicating the absence of transsulfuration pathway in MEFs, and further suggesting homocysteine-inhibited ferroptosis does

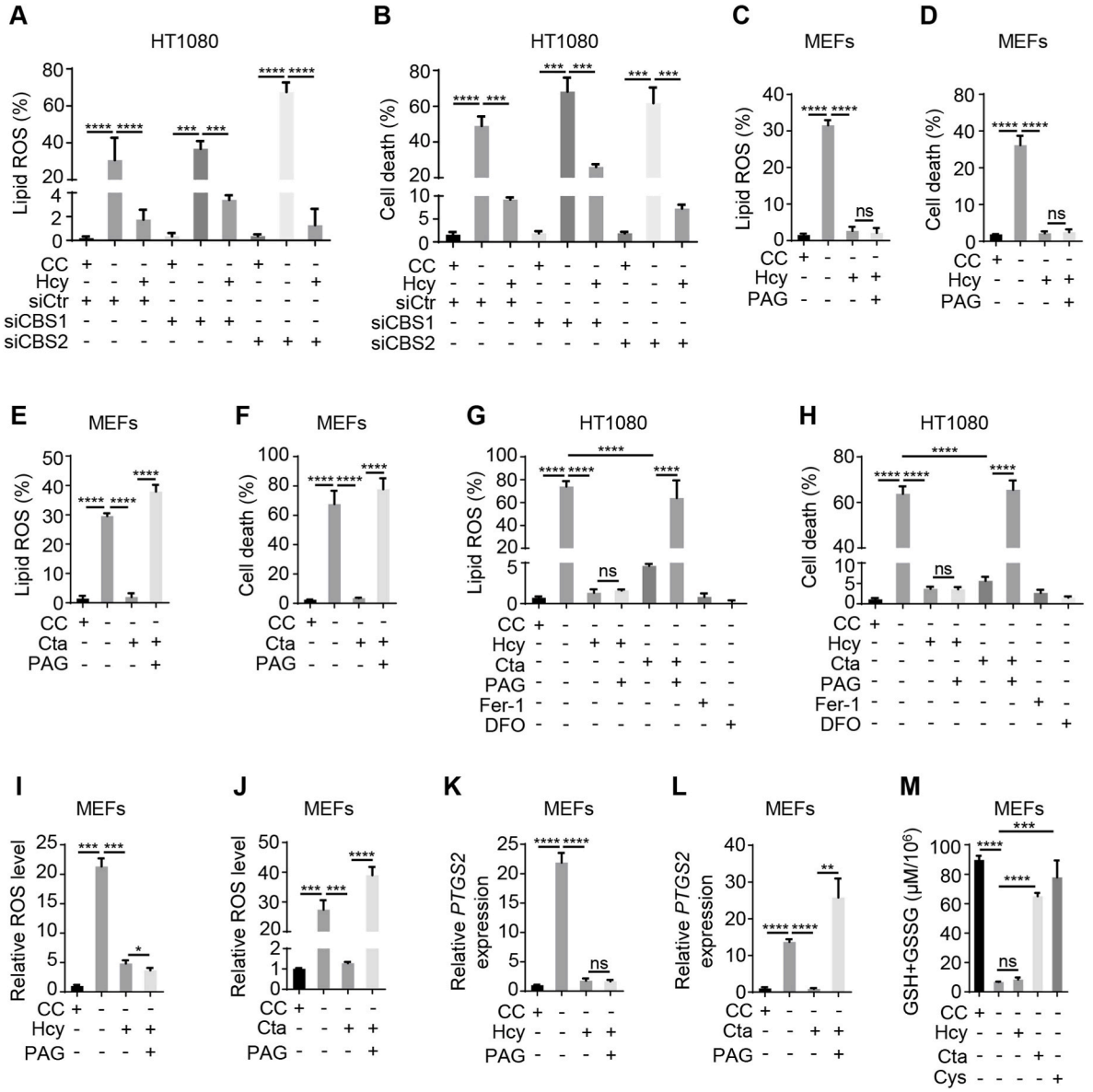

Fig. 3. The role of homocysteine in ferroptosis inhibition is independent of transsulfuration pathway

(A and B) Evaluation of lipid ROS and cell death for cystathionine β-synthase (CBS)-depleted cells. Wild type or CBS-knockdown HT1080 cells were cultured with or without cystine (CC, 400 μM) and homocysteine (Hcy, 400 μM) as indicated. Following 10 or 14 h incubation, cells were subjected to detection of lipid ROS (A) as described in Fig. 1 (B), or measurement of cell death (B) as described in Fig. 1 (C) respectively. (C and D) Evaluation of lipid ROS and cell death for cystathionine γ-lyase (CTH) inhibition in MEFs. MEFs were treated with homocysteine (Hcy, 400 μM) or (and) DL-propargylglycine (PAG, 100 μM), a chemical CTH inhibitor, in the absence of CC as indicated. Cells were treated for 8 h for analysis of lipid ROS (C) as described in Fig. 1 (B), or for 12 h for evaluation of cell death (D) as described in Fig. 1 (C). (E and F) Assessment of the effect of cystathionine (Cta) on lipid ROS and cell death in CTH-inhibited MEFs. MEFs were treated with Cta (400 μM) or/and PAG (100 μM) in the absence of CC as indicated. Lipid ROS (E) or cell death (F) were evaluated after treatment for 8 h or 12 h respectively as described in Fig. 1 (B and C). (G and H) Measurement of lipid ROS and cell death induced by Hcy (400 μM), Cta (400 μM) or PAG (400 μM) in the absence of CC. In the context of different reagent combinations as indicated, HT1080 cells were cultured for 8 h for lipid ROS determination (G) as described in Fig. 1 (B) or for 12 h for evaluation of cell death (H) as described in Fig. 1 (C). Treatment of ferroptosis inhibitor Fer-1 (10 μM) or DFO (80 μM) was the negative control. (I and J) Analysis of ROS production for Hcy or Cta treatment with or without PAG in MEFs. In the absence of CC, MEFs were cultured with Hcy (400 μM) (I), Cta (400 μM) (J) or combined with PAG (100 μM). Following 8 h incubation, cells were subjected to evaluation of ROS production. The accumulation of ROS was assayed by DCFH-DA staining coupled with flow cytometry analysis. (K and L) Evaluation of *prostaglandin-endoperoxide synthase-2* (*Ptgs2*) transcription in response to Hcy (K) or Cta (L) treatment with or without PAG in MEFs. MEFs were cultured as described in Fig. 3 (I and J) for 8 h, the mRNA level of *Ptgs2* was determined by real-time qPCR. (M) Assay of the impact of Hcy, Cta or cysteine (Cys) on glutathione (GSH) and oxidized glutathione (GSSG) level. MEFs were treated with Hcy (400 μM), Cta (400 μM), and Cys (400 μM) for 8 h in the absence of CC as indicated and subjected to measurement of GSH and GSSG level. Data represent as mean ± SD of three independent experiments, with significance determined by one-way ANOVA test. $^{*}P < 0.05$; $^{**}P < 0.01$; $^{***}P < 0.001$; $^{****}P < 0.0001$; ns, nonsignificant.

not rely on CBS. Together, these data suggested that homocysteine plays an inhibitory role in cystine deprivation-induced ferroptosis, that might directly result from the thiol group of homocysteine.

In addition to CBS, CTH is another key enzyme of transsulfuration pathway. To further clarify the function of CTH-associated catalyzation step in homocysteine-inhibited ferroptosis, we introduced CTH inhibitor, namely DL-propargylglycine (PAG), into our analysis. As expected, the inhibitory effect of homocysteine on ferroptosis (lipid ROS and cell death) was not compromised by the inactivation of CTH caused by PAG (Fig. 3C and Fig. S3 E; Fig. 3 D and Fig. S3 F). Cystathionine, the product of CBS and the substrate for CTH, was able to inhibit cystine deprivation-induced ferroptosis (lipid ROS and cell death) in MEFs too; however, this inhibitory effect can be abrogated by PAG (Fig. 3 E and Fig. S3 G; Fig. 3 F and Fig. S3 H). Likewise, in HT1080 cells, the inhibitory effect of cystathionine on ferroptosis was weakened by PAG, whereas that of homocysteine cannot be alleviated at all (Fig. 3 G and Fig. S3 I; Fig. 3H and Fig. S3 J). In parallel, we tested the effect of homocysteine on ROS, and found that homocysteine could inhibit cystine starvation-induced ROS accumulation in MEFs even with treatment of PAG, whereas the inhibitory of cystathionine was blocked by PAG (Fig. 3 I and J), indicating an inhibitory role for homocysteine in ferroptosis prevention through a non-transsulfuration pathway. Prostaglandin-endoperoxide synthase-2 (Ptgs2) is also a key marker of ferroptosis in vivo [6,27,28] and our data showed that inhibition of the transsulfuration pathway by PAG did not weaken the inhibitory effect of homocysteine on *Ptgs2* expression but the effect of cystathionine was compromised by PAG (Fig. 3 K and L). In addition, we found that homocysteine failed to be converted into GSH due to the lack of a transsulfuration pathway caused by the absence of CBS in MEFs, but cystathionine and cysteine could be used by cells to synthesize GSH (Fig. 3 M). Collectively, these data suggested that the inhibitory effect of homocysteine on cystine starvation-induced ferroptosis is independent of transsulfuration pathway.

3.4. Cysteine and homocysteine inhibit ferroptosis by serving as the substrates for GPX4

The results that cysteine and homocysteine suppressed ferroptosis in the absence of GSH synthesis spontaneously raised a question as that whether they may act as substrates of GPX4 in ferroptosis inhibition. To test, we investigated the roles of cysteine and homocysteine in GPX4 inhibitor RSL3-induced ferroptosis. As expected, we found that with the increase of RSL3 concentration, the level of lipid ROS in MEFs and the rate of cell death gradually increased, but the presence of cysteine cannot suppress lipid ROS accumulation and cell death upon RSL3 treatment (Fig. 4 A and B). We also observed that the RSL3-induced lipid ROS accumulation and cell death with A549 cells were unchanged despite the existence of cysteine (Fig. S4 A and B). In addition, overexpression of SLC7A11 (Fig. S4 C), supposed to increase the intracellular level of cysteine, also failed to hinder lipid ROS accumulation and cell death induced by RSL3 treatment in HT1080 cells (Fig. S4 D and E). Furthermore, blocking the conversion from cysteine to GSH by BSO did not arrest the upregulated lipid ROS and cell death upon RSL3 stimulation in HT1080 cells (Fig. S4 F and G). Likewise, homocysteine did not inhibit RLS3-triggered lipid ROS generation both in HT1080 cells and MEFs (Fig. 4C and D), accordingly, RLS3-induced cell death cannot be inhibited by homocysteine (Fig. 4 E and F). These data suggested the inhibitory effect of cysteine and homocysteine on ferroptosis relies on GPX4 activity.

Given that the cysteine-based ferroptosis amelioration through assisting the synthesis of persulfides has been illustrated with long-term of GPX4 genetic deletion in Pfa1 cells [29], the involvement of this pathway in short-term of GPX4 inhibition with RSL3 was evaluated. We observed that the intracellular hydrogen sulfide (H_2S) was unchanged by depletion of cysteine (Fig. S4 H); in addition, elevating the intracellular H_2S by supply of sodium hydrosulfide (NaSH) in the absence of cysteine failed to rescue ferroptotic cell death induced by treatment of RSL3 in HT1080 cells (Fig. S4 H-J). The results indicated that there was no "cysteine/persulfides" axis actualizing ferroptosis prevention, which might be explained as that a short-term GPX4 inhibition was insufficient to dictate cells to orchestrate the pathways for cysteine-based persulfides production in HT1080 cells.

Because GSH is the classical substrate for GPX4, the association strength of GSH, cysteine and homocysteine on GPX4 was evaluated by molecular docking analysis. Notably, the formation of the complex between GPX4 and cysteine (Fig. 4 H) or homocysteine (Fig. 4 I) was also evidently exhibited although not as affinitive as that between GPX4 and GSH (Fig. 4 G). Furthermore, we calculated the binding energy between GPX4 and three substrates, which is reversely related with the binding affinity. Among the three substrates, GSH had the highest affinity with GPX4 (−5.744 kcal/mol) (Fig. 4 J), whereas the affinities of GPX4 with cysteine (−3.516 kcal/mol) and homocysteine (−3.698 kcal/mol) were lower than that with GSH (Fig. 4 J), but still revealed a potential interaction of them with GPX4. Next, we explored whether GPX4 could directly utilize cysteine or homocysteine for clearing peroxides. In the in vitro GPX4 activity assay, the GPX4 activity in the presence of GSH was 8.09 ± 0.066 mU/mg; whereas, upon addition of cysteine or homocysteine, GPX4 activity was 3.07 ± 0.065 mU/mg or 5.39 ± 0.059 mU/mg, respectively (Fig. 4 K), which was in line with the result of the binding energy revealed by molecular docking analysis (Fig. 4 J). These data implied that cysteine and homocysteine are novel substrates for GPX4 and able to play an important role in GPX4-associated ferroptosis inhibition.

3.5. GSH as the most suitable substrate for GPX4 might be the result of evolution

Although GPX4 has the strongest affinity with GSH (Fig. 4 J), cysteine and homocysteine can serve as substrates for GPX4 to exert their antioxidant effects in the absence of GSH (Fig. 4 H, I, and K). This promotes us to hypothesize that GPX family and the exploitation of GSH may be the result of asynchronous evolution. To prove this hypothesis, we analyzed the differences of the expression of GPX, glutamate-cysteine ligase (GCL), and glutathione synthetase (GSS) among archaea, bacteria, and eukaryote from uniport database. We found that GPX and GSH synthetases (GCL and GSS) do not always coexist in some organisms, such as *Flexibacter*, *Planctomyces sp. SH-PL62* and *Trichomonas vaginalis* (Fig. 5 A). This result implied that no intracellular GSH exits in these organisms, so that GPX has to utilize biological thiols from other molecule, such as cysteine and homocysteine, to perform the reduction reaction. Following sequence alignment, amino acid residues differences in active center were observed between human GPX4 (hGPX4) and *Flexibacter* GPX (fGPX) (Fig. 5 B). Importantly, a key amino acid residue, U46, in hGPX4 that is critical for catalyzing reaction, was replaced by C in fGPX (Fig. 5 B). Molecular docking data further indicated that GSH, cysteine, and homocysteine could form protein ligand complexes with fGPX (Fig. 5C, D and E); surprisingly, the binding affinity of fGPX with both cysteine (−5.159 kcal/mol) and homocysteine (−5.822 kcal/mol) were significantly higher than that with GSH (−3.606 kcal/mol) (Fig. 5 F). Meanwhile, we also noticed that the binding affinity of GSH with fGPX (Fig. 5 F) is more weakened compared to that with hGPX4 (Fig. 4 J), while the binding affinities of cysteine and homocysteine with fGPX (Fig. 5 F) exceeded that with hGPX4 (Fig. 4 J). Taken together, GSH as the most suitable substrate for hGPX4 might be the result of evolutionary selection of aerobic metabolism.

4. Discussion

Aberrant iron-dependent peroxidation of polyunsaturated phospholipids on cellular membranes is the major cause of ferroptosis [1,2]. Cyst(e)ine/GSH/GPX4 axis, the classical antioxidant system, plays a critical role in preventing ferroptosis via reducing phospholipid hydroperoxides to the corresponding phospholipid alcohol; however, depletion of GSH

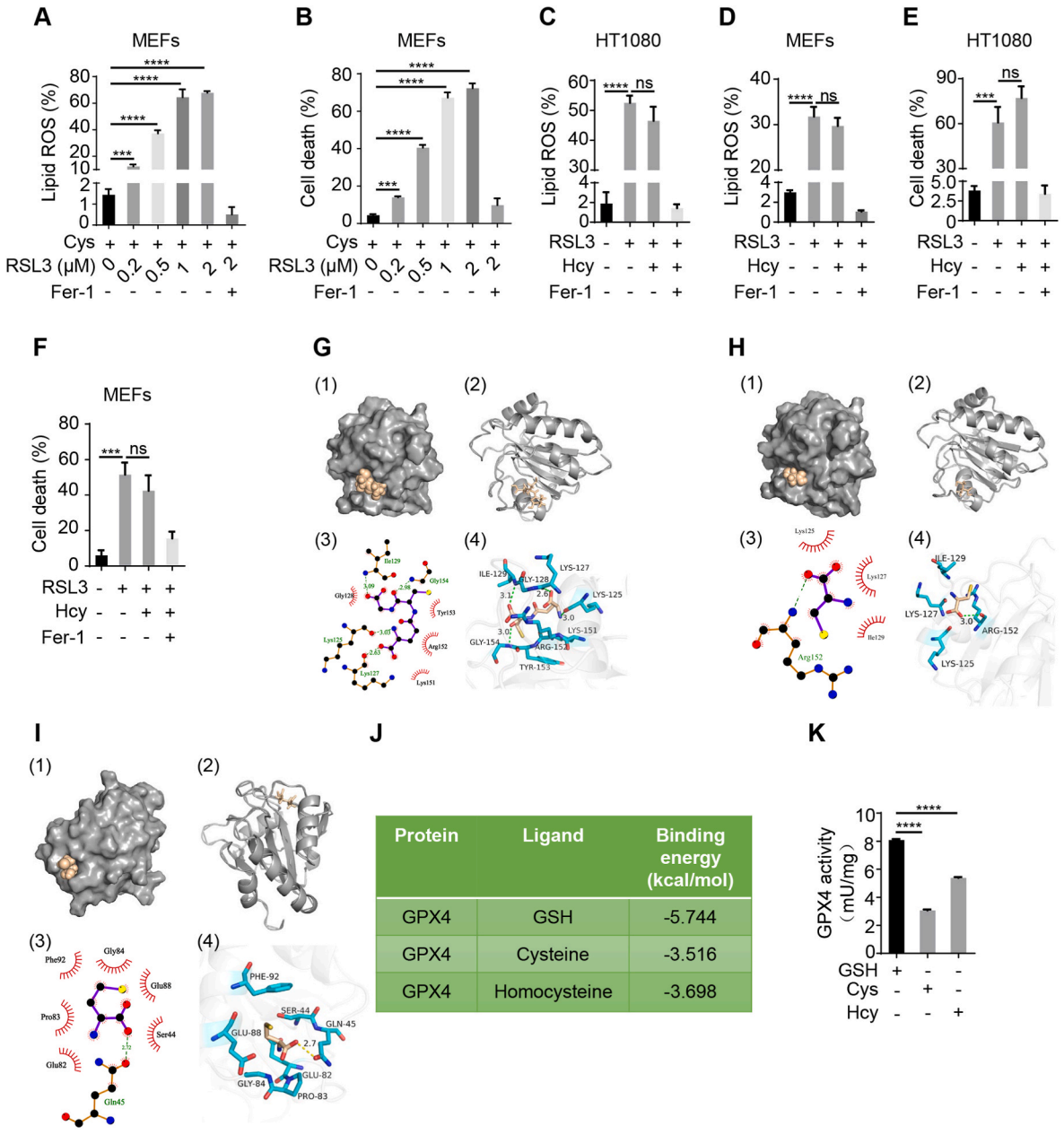

Protein	Ligand	Binding energy (kcal/mol)
GPX4	GSH	-5.744
GPX4	Cysteine	-3.516
GPX4	Homocysteine	-3.698

Fig. 4. Cysteine and homocysteine inhibit ferroptosis by serving as the substrates for GPX4.
(A and B) Evaluation of lipid ROS and cell death for GPX4 inhibition in MEFs. Cells were treated with different concentrations of GPX4 inhibitor (RSL3, 2 μM) in the presence of cysteine (Cys) as indicated. After 4 h of treatment, lipid ROS (A) was assayed as described in Fig. 1 (B). Following 8 h incubation, cells were collected and subjected to evaluation of cell death (B) as described in Fig. 1 (C). (C and D) Assessment of lipid ROS for GPX4 inhibition or/and homocysteine (Hcy) treatment. HT1080 cells (C) and MEFs (D) were treated with RSL3 (2 μM) or in the presence of Hcy (400 μM) for 4 h, and subject to evaluation of lipid ROS as described in Fig. 1 (B). (E and F) Measurement of cell death in the context of GPX4 inhibition or combined with Hcy treatment. HT1080 cells (E) and MEFs (F) were treated as described in Fig. 4 (C and D) respectively for 8 h, cell death was determined as described in Fig. 1 (C). Treatment of ferroptosis inhibitor Fer-1 (10 μM) was the negative control. (G) Molecular docking analysis of binding pattern between GPX4 and GSH. Molecular surface of GPX4 in the region of GSH binding site in (1) and (2). Schematic drawing of the interaction between GSH and GPX4 in (3) and (4). Lys 125, Lys 127, Ile 129, and Gly 154 in the active cavity of GPX4 are key amino acid residues, which take responsibility for hydrophobic interaction between GSH and GPX4. (H) Molecular docking analysis of binding pattern between GPX4 and Cys. Molecular surface of GPX4 in the region of Cys binding site in (1) and (2). Schematic drawing of the interaction between Cys and GPX4 in (3) and (4). Arg 152 in the active cavity of GPX4 is key amino acid residue that is responsible for hydrophobic interactions between Cys and GPX4. (I) Molecular docking analysis of binding pattern between GPX4 and Hcy. Molecular surface of GPX4 in the region of Hcy binding site in (1) and (2). Schematic drawing of the interaction between Hcy and GPX4 in (3) and (4). Gln 45 in the active cavity of GPX4 is the key amino acid residue for the formation of hydrophobic interaction between Hcy and GPX4. (J) Binding energy analysis between GPX4 and its substrates. (K) Evaluation of GPX4 activity. Mouse liver extracts were prepared and subjected to assay of GPX4 activity in the presence of GSH (0.25 mM), Cys (0.25 mM), or Hcy (0.25 mM) as substrate respectively. Data represent as mean ± SD of three independent experiments, with significance determined by one-way ANOVA test. ***$P < 0.001$; ****$P < 0.0001$; ns, nonsignificant.

A

Domain	Organism	GCL	GSS	GPX
Archaea	*Methanopyrus kandleri*	NO	NO	NO
	Methanothermus fervidus	NO	NO	NO
	Thermococcus	NO	NO	NO
	Archaeoglobus	NO	NO	NO
	Halobacterium Salinarum	YES	YES	NO
	Methanospirillum	NO	NO	NO
Bacteria	*Flavobacterium*	YES	YES	YES
	Flexibacter	NO	NO	YES
	Planctomyces sp. SH-PL62	NO	NO	YES
	Agrobacterium	YES	YES	YES
	Rhodospirillum tenue	YES	YES	YES
	Escherichia coli	YES	YES	Non-specific
	Synechococcus	YES	YES	YES
	Chlamydia	NO	NO	NO
Eukarya	*Giardia intestinalis*	YES	YES	NO
	Trichomonas vaginalis	NO	NO	YES
	Homo	YES	YES	YES
	Arabidopsis thaliana	YES	YES	YES
	Mouse	YES	YES	YES
	Paenibacillus sp	YES	YES	YES
	Plasmodium falciparum	YES	YES	YES
	Dictyostelium discoideum	YES	YES	YES

B

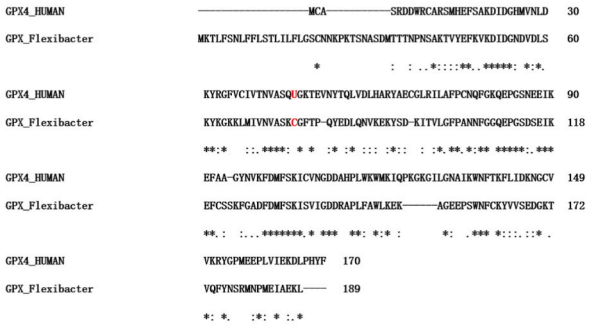

C

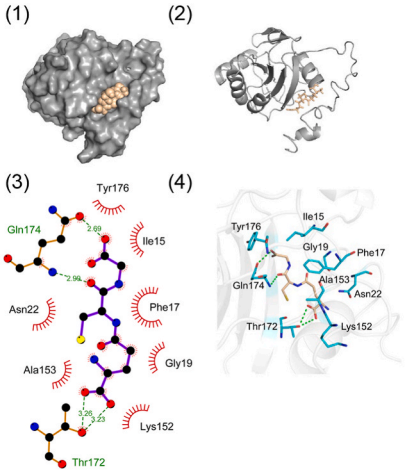

D

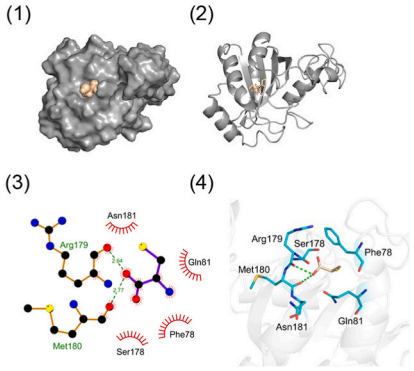

E

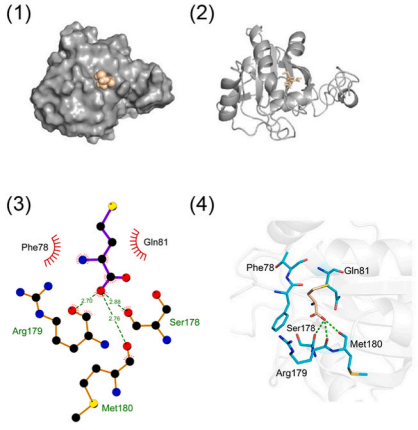

F

Protein	Ligand	Binding energy (kcal/mol)
fGPX	GSH	-3.606
fGPX	Cysteine	-5.159
fGPX	Homocysteine	-5.822

Fig. 5. GSH as the most suitable substrate for GPX4 might be the result of evolution

(A) Comparison of GPX, glutamate-cysteine ligase (GCL), and glutathione synthetase (GSS) expression in different organisms. (B) Protein sequence alignment of human GPX4 (hGPX4) and *Flexibacter* GPX (fGPX). U46 in hGPX4 were replaced by C in fGPX. (C) Molecular docking analysis of binding pattern between fGPX and GSH. Molecular surface of fGPX in the region of GSH binding site in (1) and (2). Schematic drawing of the interaction between GSH and fGPX in (3) and (4). Thr172, and Gln174 in the active cavity of fGPX are key amino acid residues, which take responsibility for hydrophobic interaction between GSH and fGPX. (D) Molecular docking analysis of binding pattern between fGPX and cysteine (Cys). Molecular surface of fGPX in the region of Cys binding site in (1) and (2). Schematic drawing of the interaction between Cys and fGPX in (3) and (4). Arg 179 and Met 180 in the active cavity of fGPX are key amino acid residues that are responsible for hydrophobic interaction between Cys and fGPX. (E) Molecular docking analysis of binding pattern between fGPX and homocysteine (Hcy). Molecular surface of fGPX in the region of Hcy binding site in (1) and (2). Schematic drawing of the interactions between Hcy and fGPX in (3) and (4). Ser 178, Arg 179, and Met 180 in the active cavity of fGPX are key amino acid residues for the formation of hydrophobic interaction between Hcy and fGPX. (F) Binding energy analysis between fGPX and its substrates.

fails to result in canonical ferroptosis [5,6]. The present study unveiled that cysteine and homocysteine can act as substrates for GPX4 to inhibit ferroptosis when the GSH synthesis pathway is blocked or absent, and GSH being chosen as the most suitable substrate for GPX4 might be a result of the evolution of aerobic metabolism.

Besides the classical antioxidant system, several GPX4-independent antioxidant systems in ferroptosis amelioration have been proposed recently. The overexpression of xCT may inhibit ferroptosis induced by genetic deletion of GPX4 due to an enhanced uptake of cysteine involves in the synthesis of persulfides [29]. In this study, the stress of genetic deletion of GPX4 might cause the re-adjustment of various metabolic genes/regulators for converting cysteine to persulfides to compensate for GPX4 lost in a context that the excessive intracellular cysteine existed. However, the effect of "cysteine/persulfides" axis was not observed in a short-term inhibition of GPX4 activity in the present study. In addition, the ferroptosis suppressor protein 1 (FSP1) suppresses ferroptosis by directly reducing the endogenous substance coenzyme Q10 (CoQ_{10}) with NAD(P)H as cofactor, which is named as NAD(P)H/FSP1/CoQ_{10} axis [30–32]. Moreover, GCH1/BH_4/DHFR and DHO/DHODH/$CoQH_2$ axes also have been illustrated with the function of anti-ferroptosis [33–35], though the contribution of DHO/DHODH/$CoQH_2$ axis seems to be context-specific [36]. Notably, the present study elucidated an inhibitory effect of cysteine or homocysteine on ferroptosis, that is GSH-independent but relies on GPX4 function. It is seemingly converse to our findings that far exceeding physiological level of homocysteine was found to be able to induce ferroptosis through inhibiting system Xc^- (sXc^-) in vascular endothelial cells [37], which may be caused by the inducible side-effect upon excessive homocysteine. Nevertheless, the function of cysteine or homocysteine acting as the substrate for GPX4 unveiled by the present study could be considered as a "cysteine or homocysteine/GPX4″ axis, which contributes to the diversity of anti-oxidation systems for the regulation of redox equilibrium, and broadens our understandings about the flexible selection of cofactors for GPX4 under different physiological or pathological conditions.

Cysteine participates in the synthesis of GSH, which is the classical substrate for GPX4. Numerous evidence suggests that depletion of cysteine through inhibiting cystine uptake, and down-regulation of GPX4 activity by RSL3, can effectively induce ferroptosis [6,9,12,13,38]; however, the synthesis process of GSH has not become an effective target for inducing ferroptosis [12]. Our data explained why depletion of intracellular GSH fails to result in ferroptosis. We found that cysteine, by superseding GSH as a GPX4 substrate, can exert inhibitory effect on ferroptosis upon the synthesis of GSH was blocked. The results of our work provide insight into the clinical observations that patients with glutathione synthase deficiency due to GCLC mutation exhibit hemolytic anemia, but have no manifestations of ferroptosis-related diseases, such as myocardial injury and neurodegenerative diseases [39–41]. The resistance of these patients from ferroptosis-related diseases might be due to that cysteine and homocysteine are used as substitutes for GSH to maintain the function of GPX4.

As the most abundant small molecule biological thiols, GSH, cysteine, and homocysteine play different roles in maintaining redox homeostasis in biological systems. It is generally believed that homocysteine can be converted to cysteine, and that cysteine, glutamate, and glycine are ligated by GCLC and GSS, producing the GSH [7]. And GSH is usually directly involved as a substrate for GPX in clearing peroxides [16]. In addition, cysteine can also participate in the synthesis of thioredoxin reductase to exert its antioxidant effect [42]. But previous work reported that GSH is found primarily in gram-negative bacteria and most eukaryotes, whereas, rarely in gram-positive bacteria [43] and a part of eukaryotes, such as *Entamoeba histolytica* [44], *Trichomonas vaginalis* [45], and *Giardia duodenalis* [46]. Despite the lack in synthetic pathway for GSH, they all possess GPX, which means that other biological thiols can maintain GPX-based redox homeostasis in GSH-free biological systems. The present study provided precise explanation by showing that cysteine and homocysteine can serve as substrates for GPX4. Additionally, during evolution, cysteine and homocysteine were present prior to GSH synthesis was developed, suggesting a shift of the substrate of GPX4 from cysteine or homocysteine to GSH. The driving force for this evolutionary selection may lie in that the organisms need to adapt to oxidative environments through the equipment of antioxidant agents such as the specialized GSH, while need cysteine to fulfill the requirement of protein synthesis. Microorganisms have been equipped with multiple unique antioxidant systems to conquer the oxidative burst imposed by environmental agents or/and phagocytic cells of the host. This enables targeting the microorganisms' antioxidant systems to be considered as a strategy for antimicrobial treatment [47–53]. The finding of the present study suggested that manipulating the unique antioxidant systems, for instance "cysteine or homocysteine/GPX" axis, might be an approach to specific control of infectious diseases, meanwhile, leaving the host's antioxidant systems unaffected.

In summary, we depict a previously unappreciated role of cysteine and homocysteine in ferroptosis inhibition. These thiol-containing molecules directly serve as a cofactor for GPX4 rather than contribute to GSH synthesis. This novel function not only shed light on multiple pathways in supporting GPX4' s function, but also suggest an evolutionary selection of GSH as the most suitable substrate for GPX4. Importantly, the discovery of the present study indicated that to inhibit or induce ferroptosis through manipulation of the intracellular cysteine or homocysteine has the clinical potential to alleviate ferroptosis-associated disease or to treat cancers and some infectious disorders.

CRediT authorship contribution statement

Chaoyi Xia: Conceptualization, Formal analysis, Investigation, Methodology, Writing - original draft. **Xiyue Xing:** Formal analysis, Investigation, Visualization. **Wenxia Zhang:** Investigation, Methodology, Visualization. **Xin Jin:** Funding acquisition, Investigation, Visualization. **Yang Wang:** Investigation, Formal analysis, Funding acquisition, Investigation. **Meihong Tian:** Conceptualization, Formal analysis, Supervision, Writing - original draft. **Xueqing Ba:** Methodology, Validation, Writing - original draft, Writing - review & editing. **Fengqi Hao:** Conceptualization, Data curation, Formal analysis, Methodology, Project administration, Supervision, Writing - original draft, Writing - review & editing.

Declaration of competing interest

The authors declare no competing interests.

Data availability

Data will be made available on request.

Acknowledgments

This work was supported by National Natural Science Foundation of China (31870896, 32101028, 32101048).

Appendix A. Supplementary data

Supplementary data to this article can be found online at https://doi.org/10.1016/j.redox.2023.102999.

References

[1] S.J. Dixon, K.M. Lemberg, M.R. Lamprecht, R. Skouta, E.M. Zaitsev, C.E. Gleason, et al., Ferroptosis: an iron-dependent form of nonapoptotic cell death, Cell 149 (2012) 1060–1072, https://doi.org/10.1016/j.cell.2012.03.042.

[2] B. Hassannia, P. Vandenabeele, T. Vanden Berghe, Targeting ferroptosis to iron out cancer, Cancer Cell 35 (2019) 830–849, https://doi.org/10.1016/j.ccell.2019.04.002.

[3] B.R. Stockwell, J.P. Friedmann Angeli, H. Bayir, A.I. Bush, M. Conrad, S.J. Dixon, et al., Ferroptosis: a regulated cell death nexus linking metabolism, redox biology, and disease, Cell 171 (2017) 273–285, https://doi.org/10.1016/j.cell.2017.09.021.

[4] G. Lei, L. Zhuang, B. Gan, Targeting ferroptosis as a vulnerability in cancer, Nat. Rev. Cancer 22 (2022) 381–396, https://doi.org/10.1038/s41568-022-00459-0.

[5] J. Zheng, M. Conrad, The metabolic underpinnings of ferroptosis, Cell Metabol. 32 (2020) 920–937, https://doi.org/10.1016/j.cmet.2020.10.011.

[6] W.S. Yang, R. SriRamaratnam, M.E. Welsch, K. Shimada, R. Skouta, V. S. Viswanathan, et al., Regulation of ferroptotic cancer cell death by GPX4, Cell 156 (2014) 317–331, https://doi.org/10.1016/j.cell.2013.12.010.

[7] M.E. Anderson, Glutathione: an overview of biosynthesis and modulation, Chem. Biol. Interact. (1998) 111–112, https://doi.org/10.1016/s0009-2797(97)00146-4, 1–14.

[8] M.H. Stipanuk, J.E.J. Dominy, J.-I. Lee, R.M. Coloso, Mammalian cysteine metabolism: new insights into regulation of cysteine metabolism, J. Nutr. 136 (2006) 1652S–1659S, https://doi.org/10.1093/jn/136.6.1652S.

[9] P. Koppula, L. Zhuang, B. Gan, Cystine transporter SLC7A11/xCT in cancer: ferroptosis, nutrient dependency, and cancer therapy, Protein Cell 12 (2021) 599–620, https://doi.org/10.1007/s13238-020-00789-5.

[10] R.J. Bridges, N.R. Natale, S.A. Patel, System xc^- cystine/glutamate antiporter: an update on molecular pharmacology and roles within the CNS, Br. J. Pharmacol. 165 (2012) 20–34, https://doi.org/10.1111/j.1476-5381.2011.01480.x.

[11] J. Lewerenz, S.J. Hewett, Y. Huang, M. Lambros, P.W. Gout, P.W. Kalivas, et al., The cystine/glutamate antiporter system xc^- in health and disease: frommolecular mechanisms to novel therapeutic opportunities, Antioxidants Redox Signal. 18 (2013) 522–555, https://doi.org/10.1089/ars.2011.4391.

[12] B.R. Stockwell, X. Jiang, The chemistry and biology of ferroptosis, Cell Chem. Biol. 27 (2020) 365–375, https://doi.org/10.1016/j.chembiol.2020.03.013.

[13] Y. Zhang, H. Tan, J.D. Daniels, F. Zandkarimi, H. Liu, L.M. Brown, et al., Imidazole ketone erastin induces ferroptosis and slows tumor growth in a mouse lymphoma model, Cell Chem. Biol. 26 (2019) 623–633.e9, https://doi.org/10.1016/j.chembiol.2019.01.008.

[14] I.S. Harris, J.E. Endress, J.L. Coloff, L.M. Selfors, S.K. McBrayer, J.M. Rosenbluth, et al., Deubiquitinases maintain protein homeostasis and survival of cancer cells upon glutathione depletion, Cell Metabol. 29 (2019) 1166–1181.e6, https://doi.org/10.1016/j.cmet.2019.01.020.

[15] Y.P. Kang, A. Mockabee-Macias, C. Jiang, A. Falzone, N. Prieto-Farigua, E. Stone, et al., Non-canonical glutamate-cysteine ligase activity protects against ferroptosis, Cell Metabol. 33 (2021) 174–189.e7, https://doi.org/10.1016/j.cmet.2020.12.007.

[16] C.-X. Yin, K.-M. Xiong, F.-J. Huo, J.C. Salamanca, R.M. Strongin, Fluorescent probes with Multiple binding sites for the discrimination of Cys, Hcy, and GSH, Angew Chem. Int. Ed. Engl. 56 (2017) 13188–13198, https://doi.org/10.1002/anie.201704084.

[17] J. Zhu, M. Berisa, S. Schwörer, W. Qin, J.R. Cross, C.B. Thompson, Transsulfuration activity can support cell growth upon extracellular cysteine limitation, Cell Metabol. 30 (2019) 865–876.e5, https://doi.org/10.1016/j.cmet.2019.09.009.

[18] G. Takebe, J. Yarimizu, Y. Saito, T. Hayashi, H. Nakamura, J. Yodoi, et al., A comparative study on the hydroperoxide and thiol specificity of the glutathione peroxidase family and selenoprotein P, J. Biol. Chem. 277 (2002) 41254–41258, https://doi.org/10.1074/jbc.M202773200.

[19] M. Gao, P. Monian, N. Quadri, R. Ramasamy, X. Jiang, Glutaminolysis and transferrin regulate ferroptosis, Mol. Cell. 59 (2015) 298–308, https://doi.org/10.1016/j.molcel.2015.06.011.

[20] M. Gao, J. Yi, J. Zhu, A.M. Minikes, P. Monian, C.B. Thompson, et al., Role of mitochondria in ferroptosis, Mol. Cell. 73 (2019) 354–363.e3, https://doi.org/10.1016/j.molcel.2018.10.042.

[21] J. Cao, X. Chen, L. Jiang, B. Lu, M. Yuan, D. Zhu, et al., DJ-1 suppresses ferroptosis through preserving the activity of S-adenosyl homocysteine hydrolase, Nat. Commun. 11 (2020) 1251, https://doi.org/10.1038/s41467-020-15109-y.

[22] C.F. Hryc, M.L. Baker, AlphaFold2 and CryoEM: revisiting CryoEM modeling in near-atomic resolution density maps, iScience 25 (2022), 104496, https://doi.org/10.1016/j.isci.2022.104496.

[23] M.F. Sanner, Python: a programming language for software integration and development, J. Mol. Graph. Model. 17 (1999) 57–61.

[24] J.J.P. Stewart, Optimization of parameters for semiempirical methods IV: extension of MNDO, AM1, and PM3 to more main group elements, J. Mol. Model. 10 (2004) 155–164, https://doi.org/10.1007/s00894-004-0183-z.

[25] J.A. Maier, C. Martinez, K. Kasavajhala, L. Wickstrom, K.E. Hauser, C. Simmerling, ff14SB: improving the accuracy of protein side chain and backbone parameters from ff99SB, J. Chem. Theor. Comput. 11 (2015) 3696–3713, https://doi.org/10.1021/acs.jctc.5b00255.

[26] A. Prudova, Z. Bauman, A. Braun, V. Vitvitsky, S.C. Lu, R. Banerjee, S-adenosylmethionine stabilizes cystathionine beta-synthase and modulates redox capacity, Proc. Natl. Acad. Sci. U.S.A. 103 (2006) 6489–6494, https://doi.org/10.1073/pnas.0509531103.

[27] B. Yan, Y. Ai, Q. Sun, Y. Ma, Y. Cao, J. Wang, et al., Membrane damage during ferroptosis is caused by oxidation of phospholipids catalyzed by the oxidoreductases POR and CYB5R1, Mol. Cell. 81 (2021) 355–369.e10, https://doi.org/10.1016/j.molcel.2020.11.024.

[28] X. Fang, H. Wang, D. Han, E. Xie, X. Yang, J. Wei, et al., Ferroptosis as a target for protection against cardiomyopathy, Proc. Natl. Acad. Sci. U.S.A. 116 (2019) 2672–2680, https://doi.org/10.1073/pnas.1821022116.

[29] U. Barayeu, D. Schilling, M. Eid, T.N. Xavier da Silva, L. Schlicker, N. Mitreska, et al., Hydropersulfides inhibit lipid peroxidation and ferroptosis by scavenging radicals, Nat. Chem. Biol. 19 (2023) 28–37, https://doi.org/10.1038/s41589-022-01145-w.

[30] S. Doll, F.P. Freitas, R. Shah, M. Aldrovandi, M.C. da Silva, I. Ingold, et al., FSP1 is a glutathione-independent ferroptosis suppressor, Nature 575 (2019) 693–698, https://doi.org/10.1038/s41586-019-1707-0.

[31] K. Bersuker, J.M. Hendricks, Z. Li, L. Magtanong, B. Ford, P.H. Tang, et al., The CoQ oxidoreductase FSP1 acts parallel to GPX4 to inhibit ferroptosis, Nature 575 (2019) 688–692, https://doi.org/10.1038/s41586-019-1705-2.

[32] L.B. Pontel, A. Bueno-Costa, A.E. Morellato, J. Carvalho Santos, G. Roué, M. Esteller, Acute lymphoblastic leukemia necessitates GSH-dependent ferroptosis defenses to overcome FSP1-epigenetic silencing, Redox Biol. 55 (2022), 102408, https://doi.org/10.1016/j.redox.2022.102408.

[33] M. Soula, R.A. Weber, O. Zilka, H. Alwaseem, K. La, F. Yen, et al., Metabolic determinants of cancer cell sensitivity to canonical ferroptosis inducers, Nat. Chem. Biol. 16 (2020) 1351–1360, https://doi.org/10.1038/s41589-020-0613-y.

[34] V.A.N. Kraft, C.T. Bezjian, S. Pfeiffer, L. Ringelstetter, C. Müller, F. Zandkarimi, et al., GTP cyclohydrolase 1/tetrahydrobiopterin counteract ferroptosis through lipid remodeling, ACS Cent. Sci. 6 (2020) 41–53, https://doi.org/10.1021/acscentsci.9b01063.

[35] C. Mao, X. Liu, Y. Zhang, G. Lei, Y. Yan, H. Lee, et al., DHODH-mediated ferroptosis defence is a targetable vulnerability in cancer, Nature 593 (2021) 586–590, https://doi.org/10.1038/s41586-021-03539-7.

[36] E. Mishima, T. Nakamura, J. Zheng, W. Zhang, A.S.D. Mourão, P. Sennhenn, et al., DHODH inhibitors sensitize to ferroptosis by FSP1 inhibition, Nature 619 (2023) E9–E18, https://doi.org/10.1038/s41586-023-06269-0.

[37] J. Shi, S. Zhang, D. Chen, S. Li, Z. Wang, Homocysteine induces ferroptosis in endothelial cells through the systemXc^-/GPX4 signaling pathway, BMC Cardiovasc. Disord. 23 (2023) 1–7, https://doi.org/10.1186/s12872-023-03342-4.

[38] M.A. Badgley, D.M. Kremer, H.C. Maurer, K.E. DelGiorno, H.-J. Lee, V. Purohit, et al., Cysteine depletion induces pancreatic tumor ferroptosis in mice, Science 368 (2020) 85–89, https://doi.org/10.1126/science.aaw9872.

[39] I. Guney Varal, P. Dogan, O. Gorukmez, S. Dorum, A. Akdag, Glutathione synthetase deficiency: a novel mutation with femur agenesis, Fetal Pediatr. Pathol. 39 (2020) 38–44, https://doi.org/10.1080/15513815.2019.1627627.

[40] P. Kaur, C. Chaudhry, I. Panigrahi, P. Srivastava, A. Kaur, Gas chromatography mass spectrometry aided diagnosis of glutathione synthetase deficiency, Lab. Med. 53 (2022) e59–e61, https://doi.org/10.1093/labmed/lmab084.

[41] V.P. Wellner, R. Sekura, A. Meister, A. Larsson, Glutathione synthetase deficiency, an inborn error of metabolism involving the gamma-glutamyl cycle in patients with 5-oxoprolinuria (pyroglutamic aciduria), Proc. Natl. Acad. Sci. U.S.A. 71 (1974) 2505–2509, https://doi.org/10.1073/pnas.71.6.2505.

[42] E.S. Arnér, A. Holmgren, Physiological functions of thioredoxin and thioredoxin reductase, Eur. J. Biochem. 267 (2000) 6102–6109, https://doi.org/10.1046/j.1432-1327.2000.01701.x.

[43] S.D. Copley, J.K. Dhillon, Lateral gene transfer and parallel evolution in the history of glutathione biosynthesis genes, Genome Biol. 3 (2002), https://doi.org/10.1186/gb-2002-3-5-research0025 research0025.

[44] R.C. Fahey, G.L. Newton, B. Arrick, T. Overdank-Bogart, S.B. Aley, *Entamoeba histolytica*: a eukaryote without glutathione metabolism, Science 224 (1984) 70–72, https://doi.org/10.1126/science.6322306.

[45] J.E. Ellis, N. Yarlett, D. Cole, M.J. Humphreys, D. Lloyd, Antioxidant defences in the microaerophilic protozoan *Trichomonas vaginalis*: comparison of metronidazole-resistant and sensitive strains, Microbiol. 140 (1994) 2489–2494, https://doi.org/10.1099/13500872-140-9-2489.

[46] D.M. Brown, J.A. Upcroft, P. Upcroft, Cysteine is the major low-molecular weight thiol in *Giardia duodenalis*, Mol. Biochem. Parasitol. 61 (1993) 155–158, https://doi.org/10.1016/0166-6851(93)90169-x.

[47] C. Staerck, A. Gastebois, P. Vandeputte, A. Calenda, G. Larcher, L. Gillmann, et al., Microbial antioxidant defense enzymes, Microb. Pathog. 110 (2017) 56–65, https://doi.org/10.1016/j.micpath.2017.06.015.

[48] P. Miramón, C. Dunker, L. Kasper, I.D. Jacobsen, D. Barz, O. Kurzai, et al., A family of glutathione peroxidases contributes to oxidative stress resistance in *Candida albicans*, Med. Mycol. 52 (2014) 223–239, https://doi.org/10.1093/mmy/myt021.

[49] X. Shen, R. Ma, Y. Huang, L. Chen, Z. Xu, D. Li, et al., Nano-decocted ferrous polysulfide coordinates ferroptosis-like death in bacteria for anti-infection therapy, Nano Today 35 (2020), 100981, https://doi.org/10.1016/j.nantod.2020.100981.

[50] Q. Shen, M. Liang, F. Yang, Y.Z. Deng, N.I. Naqvi, Ferroptosis contributes to developmental cell death in rice blast, New Phytol. 227 (2020) 1831–1846, https://doi.org/10.1111/nph.16636.

[51] R. Radi, Oxygen radicals, nitric oxide, and peroxynitrite: redox pathways in molecular medicine, Proc. Natl. Acad. Sci. U.S.A. 115 (2018) 5839–5848, https://doi.org/10.1073/pnas.1804932115.

[52] X. Wang, L. Fan, L. Cheng, Y. Sun, X. Wang, X. Zhong, et al., Biodegradable nickel disulfide nanozymes with GSH-depleting function for high-efficiency photothermal-catalytic antibacterial therapy, iScience 23 (2020), 101281, https://doi.org/10.1016/j.isci.2020.101281.

[53] F. Mo, C. Lin, J. Lu, D. Sun, Integrating artificial DNAzymes with natural enzymes on 2D MOF hybrid nanozymes for enhanced treatment of bacteria-infected wounds, Small (2023) 1–11, https://doi.org/10.1002/smll.202307256.